Correlation between Surface Morphology and Surface Forces of Protein A Adsorbed on Mica

Satomi Ohnishi,* Masami Murata,# and Masakatsu Hato*

*Surface Engineering Laboratory, Department of Polymer Physics, National Institute of Materials and Chemical Research, Ibaraki 305, and #Formulation Technology Laboratory, Chugai Pharmaceutical Co., Tokyo 115, Japan

ABSTRACT   We have investigated the morphology and surface forces of protein A adsorbed on mica surface in the protein solutions of various concentrations. The force-distance curves, measured with a surface force apparatus (SFA), were interpreted in terms of two different regimens: a "large-distance" regimen in which an electrostatic double-layer force dominates, and an "adsorbed layer" regimen in which a force of steric origin dominates. To further clarify the forces of steric origin, the surface morphology of the adsorbed protein layer was investigated with an atomic force microscope (AFM) because the steric repulsive forces are strongly affected by the adsorption mode of protein A molecules on mica. At lower protein concentrations (2 ppm, 10 ppm), protein A molecules were adsorbed "side-on" parallel to the mica surfaces, forming a monolayer of ~2.5 nm. AFM images at higher concentrations (30 ppm, 100 ppm) showed protruding structures over the monolayer, which revealed that the adsorbed protein A molecules had one end oriented into the solution, with the remainder of each molecule adsorbed side-on to the mica surface. These extending ends of protein A overlapped each other and formed a "quasi-double layer" over the mica surface. These AFM images proved the existence of a monolayer of protein A molecules at low concentrations and a "quasi-double layer" with occasional protrusions at high concentrations, which were consistent with the adsorption mode observed in the force-distance curves.

INTRODUCTION

Recently, surface force apparatuses (SFAs) (Tabor and Winterton, 1969; Israelachvili and Adams, 1978) have been used to quantify the forces of specific and nonspecific interactions between biological materials (Leckband et al., 1992; Abe et al., 1995; Pincet et al., 1995; Kutzner et al., 1997) and to monitor in real time the adsorption process of protein molecules and the conformational changes in a single enzyme (Afshar-Rad et al., 1986; Lee and Belfort, 1989; Leckband et al., 1993). Although the SFA technique has been successfully applied to the detailed study of interactions, precise discrimination between electrostatic and steric forces is still unsettled, because both electrostatic and steric forces decay roughly exponentially in most cases. The short-range strong repulsion of steric origin can be discriminated well by fitting the measured force curves to the theoretical double-layer repulsion (Claesson et al., 1995; Kuhl et al., 1994). However, it is difficult to determine whether the observed repulsion between the swollen and inhomogeneous surfaces results from the electrostatic force or the steric force, because the position of the outer helmholtz plane (OHP), which is affected by surface morphology, is not clear on such surfaces. From this viewpoint, the information about surface morphology should be particu-larly indispensable to the precise interpretation of short-range forces between such surfaces.

The atomic force microscope (AFM) (Binnig et al., 1986) has the ability to image nonconducting surfaces with high resolution in aqueous solutions, which enables studies of a wide range of solid-liquid interfaces under the same conditions as the SFA measurements. The direct observations of surface morphology with AFM provide further proof that short-range forces observed as strong repulsion are assigned to steric forces affected by the surface structure. Luckham and Manimaaran had employed SFA and rheological measurements to bridge the gap between the nanoscopic view and the macroscopic view (Luckham and Manimaaran, 1997). In the present work, we employ the combination of SFA direct force measurements and AFM observations to provide a more complete picture of the adsorbed protein molecules on mica surfaces at various protein concentrations. We present here the relationship between surface forces and the morphology of protein A molecules adsorbed on mica surfaces.

Protein A, a cell wall constituent of *Staphylococcus aureus*, has specific binding sites to the Fc fragment region of immunogloblins from most mammalian species (Forsgren and Sjöquist, 1966; Kronvall et al., 1970), and has a highly stable three-dimensional structure over wide range of temperature and pH, and in the presence of denaturing agents (Björk et al., 1972; Sjöholm, 1975). Because of its specific high affinity for IgG and considerable stability, protein A has been extensively used for immunological studies and applications (Ghetie et al., 1978; Goding, 1978; Lindmark et al., 1983; Jones et al., 1980; MacKintosh et al., 1983).

From these viewpoints, the adsorbed layer of protein A is expected to be a good substrate for binding IgG molecules

with a free Fab fragment. Therefore, as the initial stage in fabricating the protein A-IgG system, the behavior of protein A molecules during adsorption onto mica surfaces must be understood. In addition, the elongated shape of protein A is advantageous for the determination of their orientation with AFM and SFA.

Instead of using protein A originating from *Staphylococcus aureus* (hereafter referred to as SPA), our work was performed using recombinant protein A (hereafter referred to as rPA), because rPA can be obtained with less proteinaceous contaminant than SPA (Colbert et al., 1984).

A schematic drawing of the most probable structure of rPA (the model of SPA is adapted for rPA) is shown in Fig. 1 (Sjödahl, 1977a; Guss et al., 1984). rPA has a molecular weight of ~45,000 and consists of 409 amino acid residues. As with native SPA, rPA is composed of a single polypeptide chain arranged in two structurally and functionally different regions (Sjödahl, 1977a,b). The N-terminal part exhibits five homologous IgG-binding units (E, D, A, B, and C), each containing 56–61-amino acid residues (Colbert et al., 1984; Sjödahl, 1977a,b). The amino acid sequences of the five IgG-binding units of rPA and SPA are highly homologous (>95%), so that rPA retains the specific binding ability corresponding to the Fc region. The C-terminal part, region X′, consisting of 93 amino acids, corresponds to region X, the cell-wall-attachment part of SPA, which has no IgG-binding activity (Sjödahl, 1977a; Guss et al., 1984). Region X′ has a structure different from that of the IgG-binding units and has a very elongated shape similar to that of SPA (Sjödahl, 1977a,b; Guss et al., 1984). Both ends of the primary sequence (S and S′ in Fig. 1) are signal peptides consisting of 18 and 7 amino acid residues, respectively.

The schematic structure of fragment B with the C^α-chain folding model overlaid, which is based on the crystallographic data (Deisenhofer, 1981), is also shown in Fig. 1. Fragment B is composed of three helical structures arranged parallel to each other, in a triangular array with a length of ~2.6 nm and a diameter of 1.6 nm (Deisenhofer, 1981; Torigoe et al., 1990). Considering the electron density profile that is assigned to the relevant amino acid residues (Deisenhofer et al., 1978), fragment B can be viewed as a cylinder with a diameter of ~2.5 nm and a length of ~4.5

nm. Fragment B has flexible N- and C-terminal regions (the N- and C-termini 120–122 and 166–177, respectively), which may serve as flexible links to the neighboring IgG-binding units. Because the conformations of the other IgG-binding units, E, D, A, and C, are similar to that of fragment B, an rPA molecule can be taken as a rodlike molecule composed of a tandem of five globular domains. Therefore, the fully extended length of the molecule, including region X′, is expected to be 20–30 nm.

In this report, SFA measurements and AFM imaging have been used to elucidate the surface morphology, thickness, and softness of the rPA layer adsorbed on a mica surface at various protein concentrations. Based on these results and the features of rPA described above, we have proposed the mode of adsorption and the orientation of rPA molecules adsorbed on mica at each protein concentration.

MATERIALS AND METHODS

Materials

Recombinant protein A (Wako Pure Chemicals Ind., Tokyo) was used as received. According to the manufacturer, the purity is more than 98%, and its isoelectric point is pH 5.0 ± 0.1. Brown Muscovite mica (Bihar, India; a clear and slightly stained grade) was used as the substrate (Watanabe Shoko Co., Tokyo).

The rPA was diluted with a solution of sodium chloride to final concentrations of 2, 10, 30, and 100 ppm. The rPA solutions were adjusted to pH 5.0 with dilute hydrochloric acid, while keeping the total ionic strength constant (1 mM). To remove adventitious colloidal substances included in the salts, an extra-pure grade NaCl was roasted at 700°C for 8 h (Pashley, 1981; Pashley and Israelachvili, 1981). Analytical reagent-grade HCl was used in this study.

The water was purified by the following procedure. Water was first treated with the water purification system designed by our institute (reverse osmosis, ion exchange, and filtration through a 0.22-μm filter), then distilled in an all-glass apparatus. The distilled water was further distilled in an all-Pyrex still under a pure nitrogen atmosphere.

Force measurements

Force measurements were made with a Mark II surface force apparatus (Israelachvili and Adams, 1978). Details of the SFA technique have been described previously (Israelachvili, 1973; Israelachvili and Adams, 1978). The force $F(D)$ was measured as a function of distance D between two crossed mica sheets (1–4-μm thickness), which were back-silvered and glued onto cylindrical silica discs. The forces $F(D)$ between mica surfaces were measured from the deflection of a variable cantilever spring that supports the lower surfaces. The separation between surfaces was determined interferometrically by using fringes of equal chromatic order (FECO) (Israelachvili, 1973; Tolansky, 1970). The distance D between surfaces was controlled by a series of coarse and fine micrometers, with a synchronous motor coupled by a cantilever spring to the other surface.

$F(D)$, normalized by the local geometric mean radius R, is related to the free energy of interaction per unit surface area between flat surfaces G, according to the Derjaguin approximation (Derjaguin, 1934),

$$F(D)/R = 2\pi G(D) \qquad (1)$$

This approximation is valid provided that $D \gg R$, which is the case in the experiments reported here.

The detailed experimental procedure for the force measurements on rPA has been described previously (Hato et al., 1996). Before measuring the forces between rPA adsorbed on mica, we measured the forces in a solution
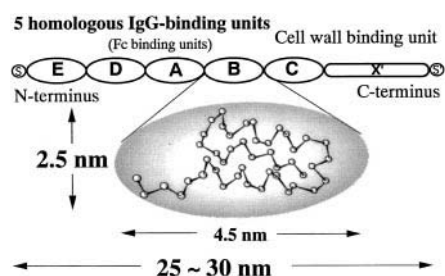

FIGURE 1 Schematic drawings of recombinant protein A (adapted from Sjödahl, 1977a) and fragment B, following the electron density map (Deisenhofer et al., 1978).

of sodium chloride (1 mM, pH 5) without rPA, and determined the contact position ($D = 0$). In this system, the measured force-versus-distance curve was identical to that predicted by Derjarguin-Landau-Verwey-Overbeek (DLVO) theory. Then the rPA solution was injected to replace the solution of sodium chloride and incubated for 24 h on mica surfaces at pH 5, which is equal to the isoelectric point of rPA. To facilitate the adsorption, the surfaces were separated by ∼1 mm during the incubation. All experiments were carried out in a room thermostatted to 22° ± 0.3°C.

Sample preparation for AFM imaging

The rPA solutions were prepared in the same manner as the solution for the force measurements. The mica substrates, which are partly covered by another piece of mica, were immersed in rPA solutions (2 ppm, 10 ppm, 30 ppm, 100 ppm in 1 mM NaCl at pH 5), as illustrated in Fig. 2. Each rPA solution was incubated for 24 h on the mica at the pH equal to the isoelectric point (pH 5) of rPA. Before the mica substrates were removed from the rPA solutions, the rPA solutions were diluted with NaCl solution (1 mM, pH 5) until the rpA concentration was less than 0.1 ppm. The rPA-adsorbed mica surfaces were slightly hydrophobic ($\theta = 30°$). The covered mica was removed just before imaging. The boundary between the adsorbed rPA layer and the mica surface was imaged to estimate the thickness of the rPA layer.

AFM imaging

The AFM system used in this study was a commercially available Nano-Scope II or IIIa (Digital Instruments, Santa Barbara, CA). The D-scanner, with a scan range of ∼12 × 12 μm, was used. The 200-μm-long cantilevers, with a nominal spring constant of 0.021 N/m and Si_3N_4 tips, were purchased from Olympus Optical Co. (Tokyo). AFM images (400 × 400 pixels) were obtained using the "height mode," which kept the force constant, at room temperature. Typical AFM parameters were as follows: integral gain = 3; proportional gain = 5; two-dimensional gain = 0.3; scan rate = 19.6 Hz; scan width = 5000–8000 nm. To obtain the best imaging conditions, the applied force was minimized and stabilized by adjusting the height of the cantilever (set point voltage) during scanning of the sample surface.

In images of larger areas (10 μm × 10 μm), the AFM images observed in air exhibited features similar to those observed in the solution of sodium chloride (1 mM, pH 5). Therefore, AFM images presented here of the boundary between the rPA layer and bare mica were obtained in air, because imaging in air was rather more stable than imaging in solution. To observe the detailed morphology (≤3 μm × 3 μm), the adsorbed rPA layer was imaged using a fluid cell in water and in the solution. We confirmed that no significantly different feature was observed between the images taken in water and those taken in the solution. The water used for AFM imaging was treated with the same method as that used for the force measurements. The typical force acting on the surfaces during imaging was 1–2 nN in air, and 10–50 pN in aqueous solutions.
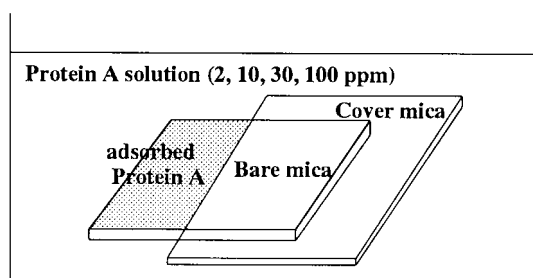

FIGURE 2 A sample of rPA molecules adsorbed on a mica substrate for AFM imaging. The rPA solution was incubated for 24 h on mica at pH 5. The covered mica was removed just before imaging.

Estimation of the amount of rPA adsorbed on mica

SFA was also employed to measure the mean refractive index (n_m) of the medium between the surfaces. We have estimated the amount of protein adsorbed per unit area (Γ) by using the approximation (Kawanishi et al., 1990)

$$\Gamma = [0.5(n_m - n_o)DN_o]/[(\partial n/\partial C)M_w] \qquad (2)$$

where Γ is expressed in the number of rPA molecules per cm^2, n_o is the refractive index of the bulk solution, D is the distance between the surfaces, N_o is Avogadro's constant, and M_w is the molecular weight of rPA (∼45,000). $\partial n/\partial C$ is assumed to be 0.19 cm^3/g, a typical value observed for many protein solutions (Timasheff, 1976).

Moreover, we have attempted to utilize AFM to estimate the adsorption density of rPA. The surface coverage and total volume of rPA adsorbed on mica were estimated from AFM images by using the "bearing analysis" function contained in the NanoScope III software.

RESULTS AND DISCUSSION

Force measurements

"Adsorbed layer" thickness, D_{ad}, and "hard wall" thickness, D_{hw}

Before describing the results of the force-distance measurements, we define two terms: an "adsorbed layer" thickness, D_{ad}, and a "hard wall" thickness, D_{hw}. When the surfaces come into contact with "jump-in" motion, D_{ad} is defined as a surface separation where the jump-in motion stops (specified on the approach curve of 30 ppm in Fig. 3). When no "jump-in" motion is observed, D_{ad} is defined as the surface separation where the force curve deviates from the exponentially repulsive curve observed at large distances (de-
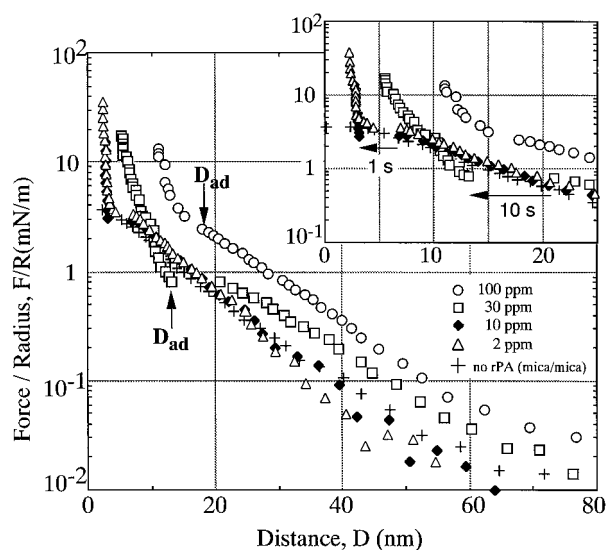

FIGURE 3 Measured forces on approach between the rPA layers incubated in various rPA concentrations at pH 5. +, Without rPA; △, 2 ppm; ◆, 10 ppm; □, 30 ppm; [○] 100 ppm. The total ionic strength was kept at 1.0 mM (NaCl + HCl). The forces without rPA can be fitted by DLVO theory ($\Psi_0 = 100$ mV, $\kappa^{-1} = 9.6$ nm, $A = 2.2 \times 10^{-20}$ J; the theoretical curve is not shown). Arrows in the inset represent the distance of "jump-in" at 30 ppm (*long arrow*), and 10 ppm (*short arrow*).

noted on the approach curve of 100 ppm in Fig. 3). D_{ad} represents the thickness of the "adsorbed layer," which is slightly compressed between the mica surfaces. D_{hw} is defined as the surface separation where the "adsorbed layer" between the mica surfaces acts as a "hard wall" with a compression load of 10–20 mN/m applied to the surfaces (Hato et al., 1996).

General features of the force curves in the presence of rPA

All of the force-distance curves in the presence of rPA can be described in terms of two different interaction regimens: a "large distance" regimen, in which an electrostatic double-layer force dominates the interactions, and an "adsorbed layer" regimen, in which forces of steric origin owing to the overlap of adsorbed layers dominate.

In the "large distance" regimen, the force is monotonically repulsive on approach with a decay length close to a theoretical Debye length for the electrolyte concentration of the medium. Therefore, the repulsive forces in this regime are predominately due to the electrostatic double-layer force originating from the charges on the surfaces of the adsorbed layers. As a first approximation, the force curves can be fitted by a DLVO-type equation,

$$F(D)/R \propto \exp(-\kappa D) \qquad (3)$$

where κ^{-1} is the theoretical Debye length.

In the small distance regimen ("adsorbed layer" regimen), the force profiles deviate significantly from the exponentially repulsive curve fitted by DLVO theory. This deviation results from steric repulsion between rPA layers. When the protein layers were compressed with 50 mN/m or more, the protein layers were plastically deformed, and they did not recover their original shape.

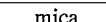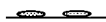On separation, the forces exhibit hysteresis, with the force minimum around the "adsorbed layer" thickness. The

maximum adhesion at 10 ppm is ~10 mN/m, and the magnitude of adhesion at higher concentrations (30 ppm, 100 ppm) is on the order of 1 mN/m. Force profiles at larger distances are identical to the approach curves. The main features of force curves are summarized in Table 1.

Force curves on approach

The forces measured on approach between the rPA layers incubated in various rPA concentrations are shown in Fig. 3. In the absence of rPA, the long-range electrostatic repulsion extends a few hundred angstroms, and at a separation of 2.2 nm, the short-range van der Waals attraction makes the surfaces jump into contact. This can be well described by DLVO theory ($\psi_o = 100$ mV, $\kappa^{-1} = 9.6$ nm).

The approach force curve of the 2 ppm exhibited the same profile as the curve for 10 ppm. In the "large distance" regimen at surface separations above 8 nm, the electrostatic repulsive force increased exponentially on compression, with a decay length of 9.6 nm, which agrees well with the Debye length for the electrolyte concentration of the medium. In the "adsorbed layer" regimen at distances smaller than 8 nm, it was observed that the surfaces jumped into contact from separations of 7–8 nm to ~3 nm (see the *inset* of Fig. 3) and approached to ~2 nm with further compression. From these results, the thickness of the "absorbed layer" (D_{ad}) and "hard wall" (D_{hw}) were found to be ~3 nm and 2 nm, respectively (i.e., $D_{hw} = 1.7 \pm 0.2$ nm at 2 ppm, $D_{hw} = 2.0 \pm 0.2$ nm at 10 ppm). Because D_{hw} is smaller than the width of the rPA molecule, a few rPA molecules are considered to be adsorbed on a mica surface with small surface coverage. Despite a few rPA molecules, the adsorption of rPA can cause the outer Helmholtz plane (OHP) to shift slightly, which is detected as the shift of "jump-in" toward larger distances.

TABLE 1   Physical properties of the rPA layers: forces and thickness of rPA adsorbed onto the mica surface at various rPA concentrations

	SFA*						AFM		
	D_{ad} (nm)	D_{hw} (nm)	Measured decay length (nm)	Surface potential (mV)	(shift) (nm)	Adhesive force on separation (mN/m)**	Height of rPA layer (nm)	Height of protrusions (nm)	Morphology of the rPA layer
0 ppm (mica/mica)	0	0	9.6	100–105	0	−50	0		mica
2 ppm	3 ± 1	1.7 ± 0.2	9.6 ± 0.1	100–105	—	−1.6 ± 0.2	1.5 ± 0.1	0	
10 ppm	3	2 ± 0.2	9.6 ± 0.2	100–105	—	−10	2.3 ± 0.1	0	
30 ppm	~13	6 ± 1	10.7 ± 0.4	90–95	6	+0.7	2.5 ± 0.2	1.5 ± 0.3	
100 ppm	~18	10 ± 1	11.1 ± 0.3	85–90	12	+1	2.5 ± 0.5	1.5 ± 0.3*** 10 ± 1****	

*, All of the values were estimated from the force curves.

**, Negative and positive signs denote attractive and repulsive regions, respectively.

***, Height of the small protrusions.

****, Total height of the rPA layer and the large protrusions.

The force profile at 30 ppm is monotonically repulsive, with a decay length of 10.7 nm in the "large distance" regimen. This long-range repulsive force is also attributed to the electrostatic force, because the force profile of the 30 ppm is in agreement with that of the medium shifted 6 nm toward larger distances ($\psi_o = 90$ mV, $\kappa^{-1} = 10.7$ nm). In the "adsorbed layer" regimen (≤ 20 nm), the surfaces jumped from ~20 nm to ~13 nm (D_{ad}). This "jump-in" motion typically took ~10 s, which was very slow compared with the 1 s required at lower rPA concentrations (2 ppm and 10 ppm). When the compression load exceeded 2.5 mN/m, the surfaces started to approach and the final surface separation was ~6 nm (at the compression load of 10 mN/m), below which the adsorbed layer in the confined space between the mica surfaces acted as a hard wall (i.e., $D_{hw} = 6 \pm 1$ nm). The starting position of the "jump-in" motion shifted slightly toward smaller distances, whereas the force profile in the "large distance" regime and D_{ad} were unchanged in subsequent compression measurements.

These results at 30 ppm strongly suggest that mica surfaces are almost covered with rPA molecules, because the thickness of the "hard wall" (6 ± 1 nm) corresponds to twice the width of an rPA molecule (2×2.5 nm). The formation of an rPA layer on mica appears to be accompanied by a 6-nm shift of the OHP toward larger distances. Because D_{ad} (13 nm) is considerably larger than D_{hw} (6 ± 1 nm), the rPA layers are considered to be quite swollen in the solution. The swollen rPA layers are reordered through confinement and release during measurements, resulting in the shifts of the starting position of the "jump-in" motion toward smaller distances.

At 100 ppm, the force curve has shifted 10–12 nm outward (toward larger distances) from that measured without rPA, and is monotonically repulsive down to ~18 nm, with a decay length of 11.1 ± 0.3 nm. At distances smaller than 18 nm (the "adsorbed layer" regimen), a significant upward deviation from the exponentially repulsive profile was observed without "jump-in" motion of the surfaces. The final "hard wall" thickness was ~10 nm, with a compression load of 10 mN/m (i.e., $D_{hw} = 10$ nm ± 1 nm), which corresponded to four times the width of an rPA molecule (4×2.5 nm).

Force curves on separation

The forces measured on separation between the rPA layers incubated in various rPA concentrations are shown in Fig. 4.

At 2 ppm, two different types of curve profile depending on the contact position were observed. One profile, which was observed more often, showed large and fast "jump-out" motion from 2 nm to more than 100 nm within 1 s (2 ppm (1) in Fig. 4). This behavior is similar to that observed between bare mica surfaces. The typical adhesive force (F/R) needed to separate the surfaces was -1.6 ± 0.2 mN/m (i.e., 1/25 of that between bare mica surfaces). The other showed a small and rather slow "jump-out" motion from 3 nm to 10 nm in 1–2 s (2 ppm (2) in Fig. 4). At
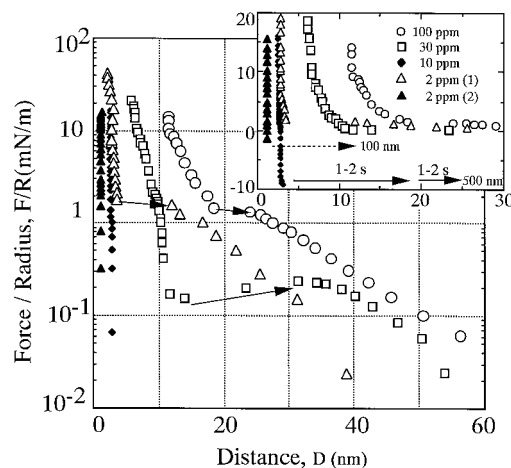

FIGURE 4 Measured forces on separation between the rPA layers incubated in various rPA concentrations at pH 5. ♦, 10 ppm; □, 30 ppm; ○, 100 ppm. Two types of force profile were observed at 2 ppm (△, ▲). The total ionic strength was kept at 1.0 mM (NaCl + HCl). Arrows represent the distance of "jump-out" at each separation. The dotted arrow represents the "jump-out" from 2 nm to more than 100 nm.

surface separations above 10 nm, the separation curve profile was identical to the approach curve profile of the 2 ppm. The depth of the force minimum $\{(F/R)_{max} - (F/R)_{min}\}$ is ~1 mN/m, which is comparable to that observed at 100 ppm. As the force profile on separation depends on the contact positions, it is thought that heterogeneous surfaces were formed on the mica by adsorption of a few rPA molecules. Therefore, the former profile is suggested to be the force profile on rPA-mica separation, and the latter profile, less commonly observed, suggests an unstable (nonequilibrium) state between surfaces at low concentrations (Claesson et al., 1995).

For the 10 ppm, a two-step "jump-out" motion was observed on separation when the adhesive force (F/R) exceeded -10 mN/m, which is five times larger than that for the 2 ppm (i.e., one-fifth of that between bare mica surfaces). The first "jump-out" motion from 4 nm to 20 nm was slow, requiring 1–2 s, and the second one from 20 nm to 500 nm was fast, occurring in 1–2 s (denoted in the *inset* of Fig. 4). This "jump-out" motion was not observed when the surfaces were withdrawn without contact. The magnitude of the adhesive force did not depend on the magnitude of the compression load from 3 mN/m to 20 mN/m, or the duration of compression from several seconds to 5 min. This suggests that the two-step "jump-out" motion originates from a "bridging" adhesive force between the rPA-mica surfaces (Israelachvili, 1991). The first slow "jump-out" motion is thought to result from the bridging of extended rPA molecules adsorbed on mica surfaces. Once the distance between surfaces exceeds a threshold value (20 nm), the second fast "jump-out" motion is observed, because of the rupture of adhesive bridges between rPA-mica surfaces.

At 30 ppm, a two-step "jump-out" motion also took place with a force minimum $\{(F/R)_{min} \approx 0.12$ mN/m$)\}$ at ~14

nm, which is close to the D_{ad} observed (~13 nm) on approach. The first "jump-out" motion was too slow to allow the range of the distinct jump to be measured (it should be from 12 nm to 14 nm). The second "jump-out" motion from 14 nm to 31 nm was also slow and took ~5 s. These slow "jump-out" motions are thought to be due to a bridging adhesive force between rPA-rPA surfaces. The depth of the force minimum $\{(F/R)_{max} - (F/R)_{min}\}$ was ~0.7 mN/m, which is smaller than that observed at 10 ppm. This also suggests that rPA-rPA contact is more dominant than rPA mica contact.

The separation curve of 100 ppm was almost the same as the approach curve. The depth of the force minimum was ~1 mN/m, which is on the same order as that of 30 ppm.

AFM imaging

General features of the adsorbed rPA layers on mica

AFM images of an rPA layer partly adsorbed on bare mica surface and histograms for the height components in each image are shown in Fig. 5, *a–d*. The dark area on the right in these images corresponds to the region of bare mica surface (height = 0). In the images of large area, the surface of the rPA layer was observed as uniformly flat surfaces at low concentrations (2 ppm, 10 ppm), and as a rather bumpy surface at a high concentration (100 ppm). The thicknesses of the adsorbed rPA layers are displayed as histograms; the average thickness is denoted by an arrow in each histogram. Clearly, the thickness of the adsorbed rPA layer increases

FIGURE 5 AFM images of the rPA layer partly adsorbed on a mica surface (*left*) and histograms of the height components in each image (*right*). Protein A molecules were adsorbed at (*a*) 2 ppm; (*b*) 10 ppm; (*c*) 30 ppm; and (*d*) 100 ppm. At 2 ppm, excess rPA molecules were adsorbed at the edge of the covered mica. Arrowheads indicate notable height components in each histogram. The area of each image is 10 μm × 10 μm. The imaging was carried out in air. The force acting on the tip was 1–5 nN.

Ohnishi et al.
Morphology and Surface Forces of Protein A
461
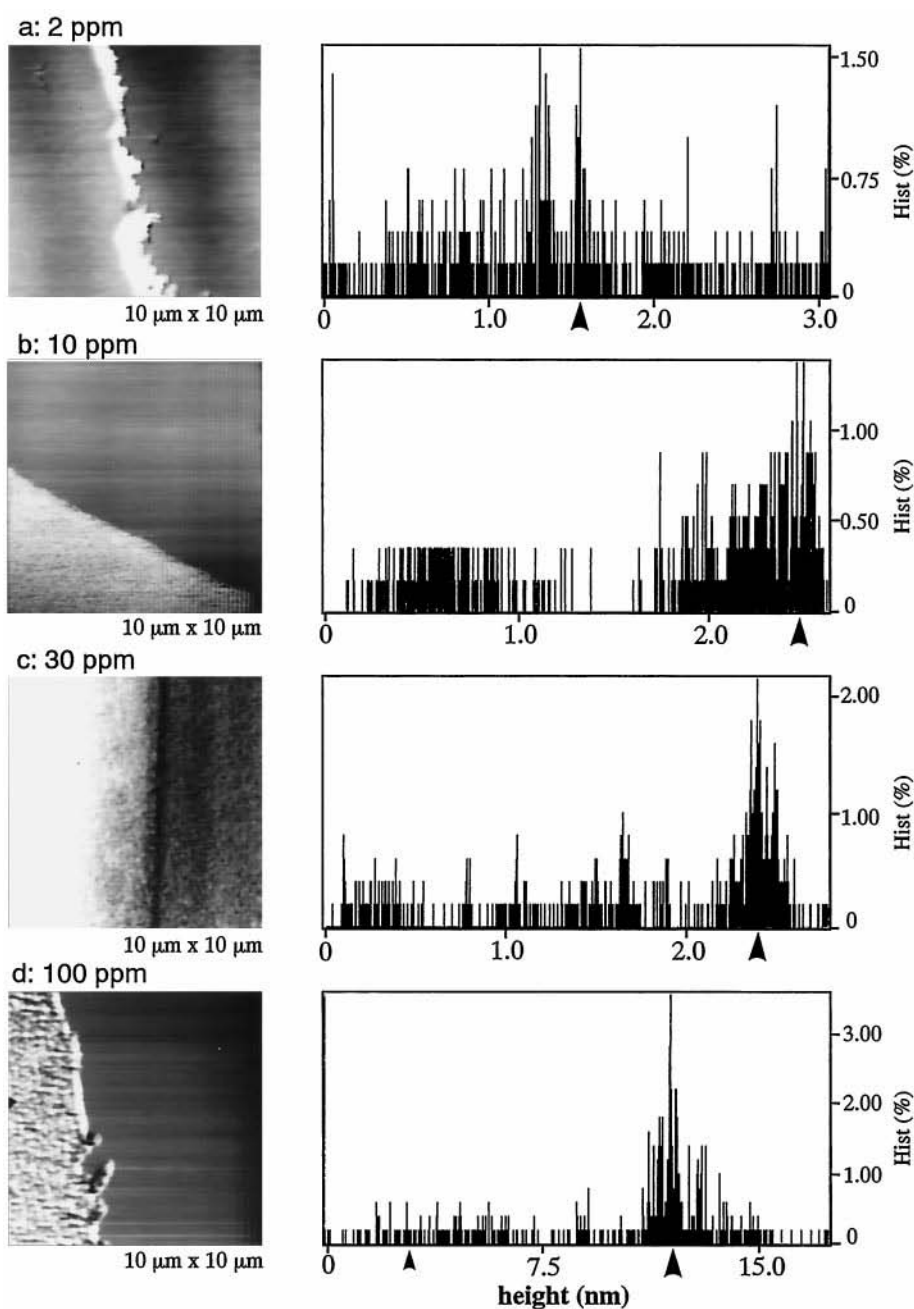
with increasing rPA concentration. The average thickness of the rPA layer adsorbed at 2 ppm (1.5 ± 0.2 nm) is less than the thickness of an rPA monolayer. It suggests that rPA molecules are adsorbed on mica with a small surface coverage. At 10 and 30 ppm, the average thickness of the rPA layers (2.3–2.5 nm) is almost equal to the thickness of the rPA molecules adsorbed side-on, parallel to the mica surfaces. These images demonstrate that, with increasing rPA concentration, the coverage of rPA to mica is increased to cover the whole mica surface, with rPA molecules adsorbed side-on, parallel to the substrate.

The surface of the rPA layer adsorbed at 100 ppm is uneven. It is observed that large protrusions ~10 nm in height are distributed over a rPA layer of 2.5–5-nm thickness (indicated by *large and small arrowheads* in the his-

togram for Fig. 5 *d*). At higher concentrations, the "side-on" adsorption should become much less preferable because of the geometric reduction of the surface area available for this adsorption. Therefore, it is thought that another type of adsorption is induced, together with the side-on adsorption. The protrusions over the rPA layer suggest that some of the adsorbed protein A molecules extended one end into the solution, whereas the remainder of each molecule adsorbed side-on to the mica surfaces.

The detailed morphology of the adsorbed rPA layer

The AFM image of rPA molecules adsorbed on mica in various rPA concentrations are shown in Fig. 6, *a–d*, with

FIGURE 6 (*Left*) AFM images of the sample of rPA molecules adsorbed on mica in various rPA concentrations. (*Right*) The height profiles (cross section) of AFM images and the schematic drawings of the possible structure of rPA based on AFM images. Five connected ovals represent one rPA molecule. Protein A molecules were adsorbed at (*a*) 2 ppm; (*b*) 10 ppm; (*c*) 30 ppm; and (*d*) 100 ppm. The image areas are (*a*, *b*) 130 nm × 130 nm; and (*c*, *d*) 3 μm × 3 μm. (*a*) Because of the "convolution effect" of the AFM tip, the length of the minor axis of the ellipsoid appeared larger than the actual size of the rPA molecule (Ohnishi et al., 1992; Vesenka et al., 1993). (*d, inset*) 1 μm × 1 μm. When the large protrusion was imaged, the small protrusions were out of focus (vague) because the AFM tip could not follow their precise topography. All of the imaging was carried out in water. The force acting on the tip was 0.1 nN or less.
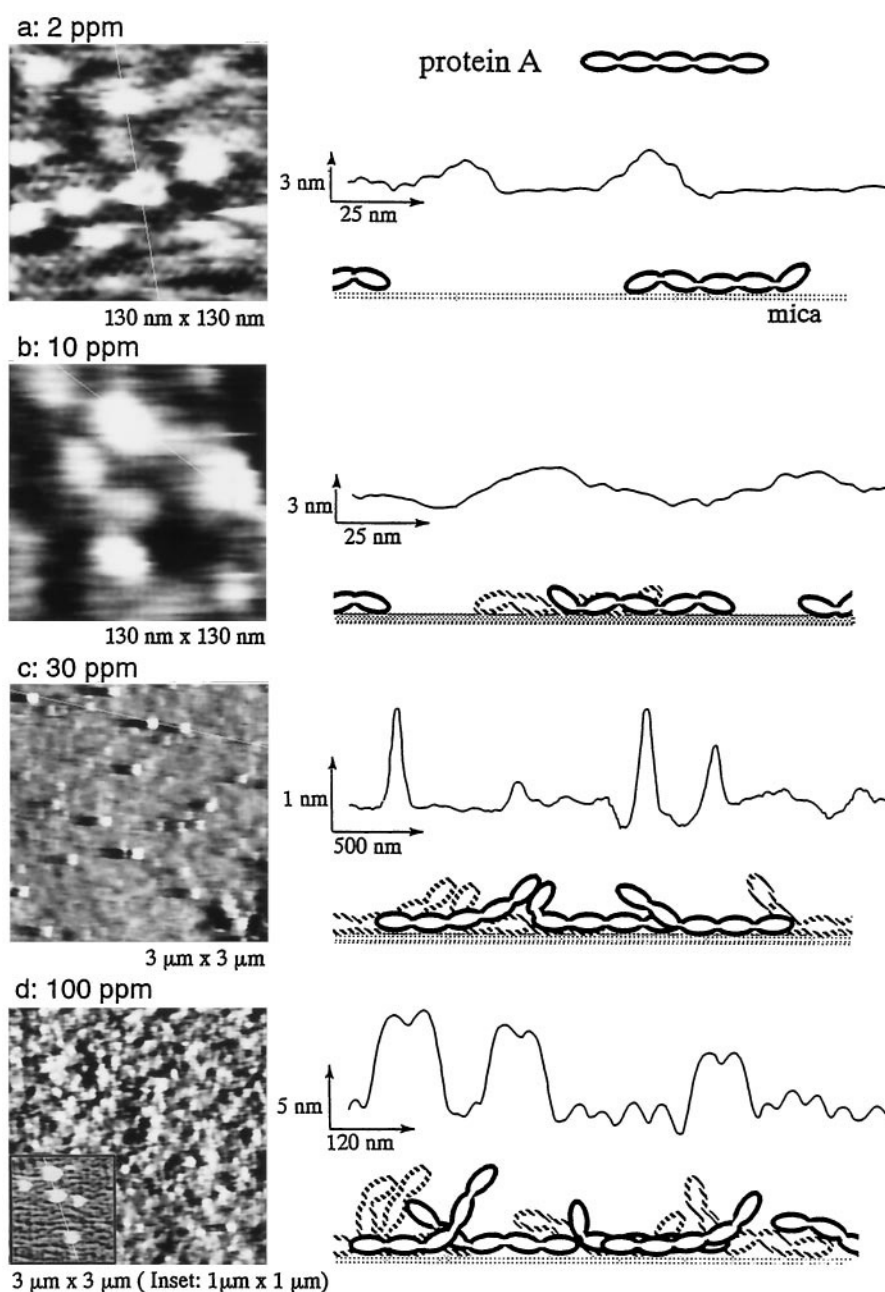
the height profiles and the schematic drawings of the possible structure of the rPA layer made according to the AFM images.

An AFM image of a sample of rPA molecules adsorbed on mica at 2 ppm is shown in Fig. 6 a. Ellipsoids are observed to be distributed randomly on the substrate in two dimensions. The apparent dimensions of the individual ellipsoid are ~25 nm (major axis) and 2.5 nm (height axis), which agree well with the size of rPA molecule. This indicates that the ellipsoids can be identified as a single rPA molecule adsorbed side-on, parallel to the mica surface. The mica lattice was observed in the regions devoid of rPA. This observation revealed that the rPA molecules were distributed randomly over the mica surface with only small surface coverage at 2 ppm.

The AFM image of the sample of rPA molecules adsorbed on mica at 10 ppm showed that the ellipsoidal objects were nonuniformly aggregated on the substrate (Fig. 6 b). The size distribution of the ellipsoidal objects, which is estimated to be ~20–40 nm, implies that the objects are aggregates of rPA molecules. The height of the aggregates was ~2.5 nm, consistent with the height of the rPA molecule adsorbed side-on to the substrate. Almost all rPA molecules should be adsorbed side-on, parallel to the mica surface at 10 ppm.

AFM images of the rPA layer at 30 and 100 ppm are shown in Fig. 6, c and d, respectively. These images exhibit the protruding structures over the rPA monolayer. At 30 ppm, the height of protrusions over the rPA layer is 1–2 nm, which suggests that the ends of the rPA molecules adsorbed side-on to the mica are on top of each other and form small protrusions (1–2 nm), because of the geometric reduction of the surface area available for this adsorption. In this condition, the number of rPA molecules adsorbed on mica is sufficient to cover the whole mica surface.

At 100 ppm, more protrusions (1–2 nm in height) were observed than at 30 ppm (Fig. 6 d), which suggests that as the rPA concentration was increased, the number of overlapping rPA molecules increased. In addition, large protrusions as observed in Fig. 5 d were also often observed (Fig.

6 d, inset). From these it is suggested that the thickness distribution in the image of large area (Fig. 5 d) is due to these protrusions. Thus, small protrusions coexist with large protrusions at 100 ppm. The average height of the protrusions was 10 nm, which is comparable to the length of two or three IgG-binding subunits. From these points, the protrusion is identified as being rpA molecules partially adsorbed on mica, with their free ends dangling from the adsorbed section of each rPA molecule. It seems that the "partial end-on" adsorption was simultaneously induced with side-on adsorption at high rPA concentrations.

Lee and Belfort had proposed the model of orientation of ribonuclease A (RNase A) on mica surfaces during adsorption (Lee and Belfort, 1989). According to their reports (Lee and Belfort, 1989; Belfort and Lee, 1991), the RNase A molecules lie flat on the mica initially, and they reorient to lie end-on, with their largest axis perpendicular to the surface as adsorption proceeds. Protein A seems to display a trend similar to that of RNase A in the adsorption process.

Possible structure of the rPA layer adsorbed on mica

D_{ad}, D_{hw}, and the height (thickness) of the adsorbed layer detected by AFM in each rPA concentration are summarized in Table 1. Clearly, D_{hw} values of 2 ppm and 10 ppm are equal to the heights of the rPA layer detected with AFM. Under these conditions, when two surfaces covered with rPA molecules come into contact, the rPA molecules intercalate to form a single rPA layer between the surfaces, because the surface coverage of the rPA molecules is sufficiently low.

At 2 ppm, it is thought that the number of rPA molecules in the confined space between mica surfaces is too small to form a stable single rPA layer, and thus the thickness of the rPA layer detected with SFA is compressed slightly (1.5–1.7 nm) and is less than the single-layer thickness (Fig. 7 a). At 10 ppm, the number of rPA molecules between the mica substrates is sufficient to form a stable single rPA layer with

FIGURE 7 Schematic illustration of the possible structure of rPA layer adsorbed at (a) 2 ppm; (b) 10 ppm; (c) 30 ppm; and (d) 100 ppm. Five connected ovals represent one rPA molecule. The illustrated configurations correspond to those at surface separations of D_{ad} (left) and D_{hw} (right).
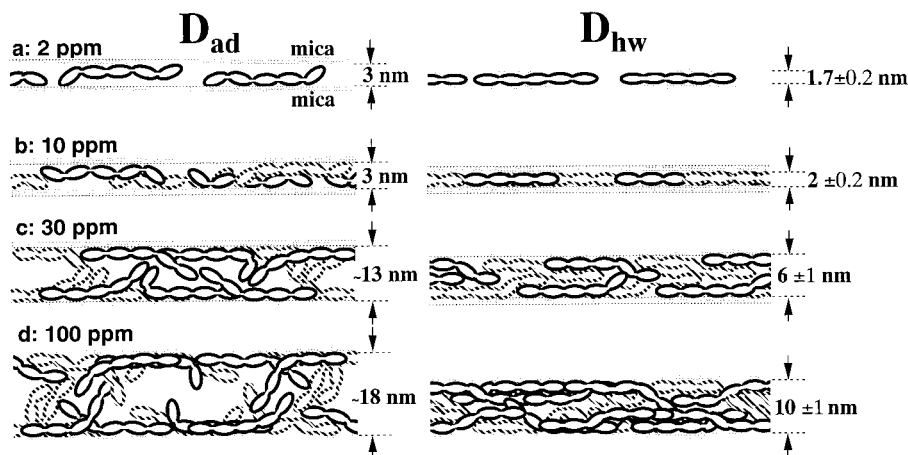
a thickness of 2–2.3 nm, corresponding to the thickness of an rPA molecule adsorbed side-on, parallel to the mica surfaces (Fig. 7 b).

At 30 ppm, the "hard wall" thickness of ∼6 nm is almost equal to twice the height of the rPA adsorbed layer and protrusions. In the force curve of the 30 ppm, the soft "wall" was detected around 13 nm (D_{ad}) before the surface separation finally reached the "hard-wall" thickness of 6 nm. At surface separations above 13 nm, the small ends of the rPA molecules, observed as protrusions, extend into the solution. The extended free ends dangling in the solution are thought to begin to touch each other when the separation gap between mica surfaces is reduced to ∼13 nm (Fig. 7 c).

The D_{hw} of 100 ppm is two or three times larger than the height of the layer and protrusions detected by AFM. As the soft "wall" was detected around 18 nm (D_{ad}), the soft "wall" appears to be composed of the extended part of rPA molecules dangling in the solution, observed as 10-nm-long protrusions in the AFM images. Assuming that the monolayer thickness of rPA molecules adsorbed side-on, parallel to the mica, is 2.5 nm, the D_{hw} of the 100 ppm corresponds roughly to four layers of rPA adsorbed side-on to the mica. From these observations, it is thought that rPA molecules form a "quasi-double layer" over the mica surface. Before compression, one end of the rPA molecule is attached to a mica surface, whereas the other end of the rPA molecule extends into the solution. In the confined space after compression, the dangling ends overlap over the adsorbed rPA layer, forming a "quasi-double layer" (Fig. 7 d). AFM images have visualized the free ends of the rPA molecules (either IgG-binding units or an X′ part) extending into the solution in this adsorption mode.

Estimating the number of rPA molecules adsorbed on mica

It is worthwhile to estimate the number of rPA molecules adsorbed onto the mica to confirm our model illustrated in Fig. 7. To estimate the number of rPA molecules adsorbed, we assume that an rPA molecule has a rod shape with a diameter of ∼2.5 nm and a length of ∼25 nm. For a close-packed monolayer where all rPA molecules are adsorbed side-on, parallel to the surface, the adsorption density of rPA is calculated to be 10^{12} to 2×10^{12} molecules/cm^2, which is comparable to the Γ (∼2.5×10^{12}) estimated from the refractive index of the rPA layer adsorbed at 30 ppm. The adsorption density of 100 ppm was also estimated to be 5.0×10^{12} molecules/cm^2, which is two times higher than that of 30 ppm. This is consistent with the model of a "monolayer" at 30 ppm, and a "quasi-double layer" at 100 ppm.

In addition, we attempted to utilize AFM to estimate the adsorption density. The estimation was carried out in the following way. The rPA layer adsorbed on mica was intentionally scratched with the tip with a strong force of 50–100 nN, which was ∼100 times stronger than the force acting on

the tip for imaging. After several scans, the rPA molecules that were swept out were aggregated at the edge of scanning area, and the mica surface was visible (Fig. 8). The number of rPA molecules was calculated by dividing the volume of the aggregation by the volume of one rPA molecule. The adsorption density was estimated from the number of rPA molecules per scratched area of mica surface.

The adsorption density estimated by AFM is summarized in Table 2. It is of interest to compare the adsorption density estimated by AFM (Γ_{AFM}) with that estimated from the refractive index (Γ_{ref}). Both estimates are on the order of 10^{12} molecules/cm^2. Furthermore, the Γ_{AFM} of 100 ppm is two times higher than that of 30 ppm, showing the same tendency as Γ_{ref}. From these points, it is clear that AFM can provide a valid estimate of the adsorption density, although there is a large margin of error, because of the assumptions involved.

The surface coverage estimated with AFM is also summarized in Table 2. The coverage at the lower rPA concentrations (2 and 10 ppm) was estimated directly from AFM images by "bearing analysis." The coverage at the higher rPA concentrations (30 and 100 ppm) was calculated using Γ_{AFM}. The incomplete surface coverages at the lower concentrations imply that rPA molecules do not cover the whole mica surface in these conditions. At 30 ppm, the surface coverage of ∼110% indicates that rPA molecules adsorbed on mica cover the whole mica surface. Furthermore, the surface coverage of 190% at 100 ppm indicates that the number of rPA molecules adsorbed on mica is slightly less than twice that at 30 ppm. This high coverage at 100 ppm is also consistent with the rPA molecules forming a "quasi-double layer" over the mica surface. Thus Γ_{ref}, Γ_{AFM} and surface coverage provide further evidence for our model.
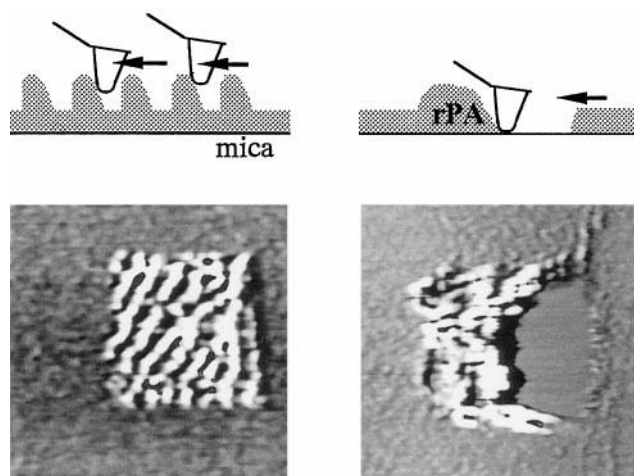

FIGURE 8   The surfaces of the rPA layer scratched by tip scanning with a strong applied force of 50–100 nN. The stripe structure is formed through the "stick-slip" of the tip on the rPA layer (*left*). The mica surface was revealed by scratching with the tip (*right*).

          Biophysical Journal   Volume 74   January 1998

TABLE 2 The amount of rPA adsorbed onto the mica surface at various rPA concentrations

Refractive index	Amount of rPA adsorbed on mica		
	Γ_{ref} ($\times 10^{12}$ molecules/cm^2)	Γ_{AFM}	Coverage* (%)
—	—	—	—
—	—	—	23 ± 5
—	—	—	52 ± 7
1.42 ± 0.02	2.5	1.7	110 ± 5
1.48 ± 0.02	5	3.3	190 ± 10

Γ_{ref}, Amount of rPA per area was estimated from the refractive index of the rPA layer at D_{hw} (molecules/cm^2).

Γ_{AFM}, Amount of rPA per area was estimated from the AFM image of the rPA layer (molecules/cm^2).

*Surface coverage was calculated by using Γ_{AFM}.

We have attributed the long-range repulsion observed in this system to an electrostatic double-layer force by fitting the measured force curves to the theoretical curve shifted toward large distances, because the OHP is shifted toward large distances as rPA molecules are adsorbed on mica. A shift of 6 nm was observed at 30 ppm (Table 1). Assuming that the shifts correspond to the position of the OHP, the OHP at 30 ppm is located at 3 nm from the mica surface. Because the thickness of a monolayer of rPA molecules adsorbed side-on to a mica surface is ~3 nm, the OHP at 30 ppm is thought to be located in the vicinity of the surface of the rPA monolayer. The small protrusions at 30 ppm do not seem to affect the position of the OHP. A shift of 12 nm was observed at 100 ppm (Table 1), so that the OHP at 100 ppm is located at 6 nm from the mica surface. Because 6 nm is larger than the sum of the height of the rPA layer and the small protrusions, and smaller than the height of the large protrusions, the OHP at 100 ppm is thought to be located in the vicinity of the surface of the small protrusions. At 100 ppm, the protrusions, mainly small ones, seemed to affect the position of the OHP. Moreover, as the number of protrusions increased, the shift of the OHP became larger, and the deviation of κ^{-1} from that of the medium (9.6 nm) also became larger.

CONCLUSIONS

The interaction force between rPA layers adsorbed on mica is mainly composed of electrostatic double-layer forces at large distances and steric repulsive force at small distances. At lower rPA concentrations (2–10 ppm), rPA molecules are adsorbed side-on to mica surfaces and tend to form a uniform monolayer. At higher concentrations, protruding structures are formed over the rPA monolayer, with the dangling end of the rPA molecules adsorbed partially end-on to mica surfaces. Using both SFA and AFM techniques, we have clarified the features of rPA layers adsorbed in various rPA concentrations and their physical properties.

REFERENCES

Abe, T., K. Kurihara, N. Higashi, and M. Niwa. 1995. Direct measurement of surface forces between monolayers of anchored poly(L-glutamic acid). *J. Phys. Chem.* 99:1820–1823.

Afshar-Rad, T., A. Bailey, P. F. Luckham, W. MacNaughtan, and D. Chapman. 1986. Direct measurement of forces between lipid bilayers. *Faraday Discuss. Chem. Soc.* 81:239–248.

Belfort, G., and C.-S. Lee. 1991. Attractive and repulsive interactions between and within adsorbed ribonuclease A layers. *Proc. Natl. Acad. Sci. USA.* 88:9146–9150.

Binnig, G., C. F. Quate, and Ch. Gerber. 1986. Atomic force microscope. *Phys. Rev. Lett.* 56:930–933.

Björk, I., B.-Å. Petersson, and J. Sjöquist. 1972. Some physicochemical properties of protein A from *Staphylococcus aureus. Eur. J. Biochem.* 29:579–584.

Claesson, P. M., E. Blomberg, J. C. Fröberg, T. Nylander, and T. Arnebrant. 1995. Protein interactions at solid surfaces. *Adv. Colloid. Interface Sci.* 57:161–228.

Colbert, D., A. Anilionis, P. Gelep, J. Farley, and R. Breyer. 1984. Molecular organization of the protein A gene and its expression in recombinant host organisms. *J. Biol. Response Mod.* 3:255–259.

Deisenhofer, J. 1981. Crystallographic refinement and atomic models of a human Fc fragment and its complex with fragment B of protein A from *Staphylococcus aureus* at 2.9- and 2.8-Å resolution. *Biochemistry.* 20:2361–2370.

Deisenhofer, J., T. A. Jones, R. Huber, J. Sjödahl, and J. Sjöquist. 1978. Crystallization, crystal structure analysis and atomic model of the complex formed by a human fragment B of protein A from *Staphylococcus aureus. Hoppe Seylers Z. Physiol. Chem.* 359:975–985.

Derjaguin, B. V. 1934. Friction and adhesion. IV. The theory of adhesion of small particles. *Kolloid Zeits. (Russia).* 69:155–164.

Forsgren, A., and J. Sjöquist. 1966. "Protein A" from *S. aureus.* I. Pseudo-immune reaction with human gamma-globulin. *J. Immunol.* 97:822–827.

Ghetie, V., G. Mota, and J. Sjöquist. 1978. Separation of cells by affinity chromatography on *Staphylococcus aureus. J. Immunol. Methods.* 21:133–142.

Goding, J. W. 1978. Use of staphylococcal protein A as an immunological reagent. *J. Immunol. Methods.* 20:241–253.

Guss, B., M. Uhlén, B. Nilsson, M. Lindberg, J. Sjöquist, and J. Sjödahl. 1984. Region X, the cell-wall-attachment part of staphylococcal protein A. *Eur. J. Biochem.* 138:413–420.

Hato, M., M. Murata, and T. Yoshida. 1996. Surface forces between protein A adsorbed mica surfaces. *Colloids Surfaces A Physicochem. Eng. Aspects.* 109:345–361.

Israelachvili, J. 1973. Thin film studies using multiple beam interferometry. *J. Colloid Interface Sci.* 44:259–272.

Israelachvili, J. 1991. Intermolecular and Surface Forces. Academic Press, London.

Israelachvili, J., and G. Adams. 1978. Measurement of forces between two mica surfaces in aqueous electrolyte solutions in the range 0–100 nm. *J. Chem. Soc. Faraday Trans. I.* 74:975–1001.

Jones, F. R., L. H. Yoshida, W. C. Ladiges, and M . A. Kenny. 1980. Treatment of feline leukemia and reversal of FeLV by ex vivo removal of IgG: a preliminary report. *Cancer.* 46:675–684.

Kawanishi, N., H. K. Christenson, and B. W. Ninham. 1990. Measurement of the interaction between adsorbed polyelectrolytes: gelatin on mica surfaces. *J. Phys. Chem.* 94:4611–4616.

Kronvall, G., H. M. Grey, and R. C. Williams, Jr. 1970. Protein A reactivity with mouse immunoglobulins. *J. Immunol.* 105:1116–1123.

Kuhl, T. L., D. E. Leckband, D. D. Laisac, and J. N. Israelachvili. 1994. Modulation of interaction forces between bilayers exposing short-chained ethylene oxide head groups. *Biophys. J.* 66:1479–1488.

Kutzner, H. B., P. F. Luckham, and J. Rennie. 1997. Measurement of the viscoelastic properties of thin surfactant films. *Faraday Discuss.* 104:9–16.

Leckband, D., Y.-L. Chen, J. Israelachvili, H. H. Wickman, M. Fletcher, and R. Zimmerman. 1993. Measurements of conformational changes

during adhesion of lipid and protein (polylysine and S-layer) surfaces. *Biotechnol. Bioeng.* 42:167–177.

Leckband, D., J. N. Israelachvili, F.-J. Schmitt, and W. Knoll. 1992. Long-range attraction and molecular rearrangements in receptor-ligand interactions. *Science.* 255:1419–1421.

Lee, S.-L., and G. Belfort. 1989. Changing activity of ribonuclease A during adsorption: a molecular explanation. *Proc. Natl. Acad. Sci. USA.* 86:8392–8396.

Lindmark, R., K. Thorén-Tolling, and J. Sjöquist. 1983. Binding of immunoglobulins to protein A and immunogloblin levels in mammalian sera. *J. Immunol. Methods.* 62:1–13.

Luckham, P. F., and S. Manimaaran. 1997. A nanorheological study of adsorbed polymer layers. *Macromolecules.* 30:5025–5033.

MacKintosh, F. R., K. Bennett, S. Shiff, J. Shields, and S. W. Hall. 1983. Treatment of advanced malignancy with plasma perfused over staphylococcal protein A. *West. J. Med.* 139:36–40.

Ohnishi, S., M. Hara, T. Furuno, and H. Sasabe. 1992. Imaging the ordered arrays of water-soluble protein ferritin with the atomic force microscope. *Biophys. J.* 63:1425–1431.

Pashley, R. M., 1981. DLVO and hydration forces between mica surfaces in lithium, sodium, potassium, and cesium ions electrolyte solutions: a correlation of double-layer and hydration forces with surface cation exchange properties. *J. Colloid Interface Sci.* 83:531–546.

Pashley, R. M., and J. N. Israelachvili. 1981. A comparison of surface forces and interfacial properties of mica in purified surfactant solutions. *Colloids Surf.* 2:169–187.

Pincet, F., E. Perez, and G. Belfort. 1995. Molecular interactions between proteins and synthetic membrane polymer films. *Langmuir.* 11:1229–1235.

Sjödahl, J. 1977a. Repetitive sequences in protein A from *Staphylococcus aureus. Eur. J. Biochem.* 73:343–351.

Sjödahl, J. 1977b. Structural studies on the four repetitive Fc-binding regions in protein A from *Staphylococcus aureus. Eur. J. Biochem.* 78:471–490.

Sjöholm, I. 1975. Protein A from *Staphylococcus aureus.* Spectropolarimetric and spectrophotometric studies. *Eur. J. Biochem.* 51:55–61.

Tabor, D., and R. H. S. Winterton. 1969. The direct measurement of normal and retarded van der Waals forces. *Proc. R. Soc. Lond. A.* 312:435–450.

Timasheff, S. N. 1976. Handbook of Biochemistry and Molecular Biology, Vol. 2, 3rd Ed. G. D. Fasman, editor. CRC Press, Cleveland.

Tolansky, S. 1970. Multiple-Beam Interferometry of Surfaces and Films. Dover, New York.

Torigoe, H., I. Shimada, A. Saito, M. Sato, and Y. Arata. 1990. Sequential ^{1}H NMR assignments and secondary structure of the B domain of staphylococcal protein A: structural changes between the free B domain in solution and the Fc-bound B domain in crystal. *Biochemistry.* 29:8787–8793.

Vesenka, J., S. Manne, R. Giberson, T. Marsh, and E. Henderson. 1993. Colloidal gold particles as an incompressible atomic force microscope imaging standard for assessing the compressibility of biomolecules. *Biophys. J.* 65:992–997.